ARTICLE

Combining magnetic nanoparticle capture and poly-enzyme nanobead amplification for ultrasensitive detection and discrimination of DNA single nucleotide polymorphisms

Received 00th January 20xx,
Accepted 00th January 20xx

DOI: 10.1039/x0xx00000x

www.rsc.org/

Lorico D. S. Lapitan Jr,[a,b] Yihan Xu,[a] Yuan Guo*[,c] and Dejian Zhou*[,a]

The development of ultrasensitive methods for detecting specific genes and discriminating single nucleotide polymorphisms (SNPs) is important for biomedical research and clinical disease diagnosis. Herein, we report an ultrasensitive approach for label-free detection and discrimination of a full-match target-DNA from its cancer related SNPs by combining magnetic nanoparticle (MNP) capture and poly-enzyme nanobead signal amplification. It uses a MNP linked capture-DNA and a biotinylated signal-DNA to sandwich the target followed by ligation to offer high SNP discrimination: only the perfect-match target-DNA yields a covalently linked biotinylated signal-DNA on the MNP surface for subsequent binding to a neutravidin-horseradish peroxidase conjugate (NAV-HRP) for signal amplification. The use of polymer nanobeads each tagged with thousands of copies of HRPs greatly improves the signal amplification power, allowing for direct, amplification-free quantification of low aM target-DNA over 6 orders of magnitude (0.001-1000 fM). Moreover, this sensor also offers excellent discrimination between the perfect-match gene and its cancer-related SNPs and can positively detect 1 fM perfect-match target-DNA in the presence of 100 fold excess of co-existing single-base mismatch targets. Furthermore, it works robustly in clinically relevant media (e.g. 10% human serum) and gives even higher SNP discrimination than that in clean buffers. This ultrasensitive DNA sensor appears to have excellent potential for rapid detection and diagnosis of genetic diseases.

Introduction

The development of sensitive DNA detection and quantification method has attracted significant research efforts due to importance in biomedical research[1-3] and clinical diagnosis[4-6]. In particular, ultrasensitive detection of single nucleotide polymorphisms (SNPs) in genetics has great potential to diagnose life-threatening illnesses (*i.e.* cancer, diabetes, vascular diseases, *etc.*), prediction of patient's response to treatments and risk of possible relapse, and therefore has been of great interest for both scientists and clinicians[7, 8]. However, disease related SNPs are often found in extremely low concentrations in an overwhelming background of wildtype gene, which can only be detected reliably after substantial amplification, making them challenging targets to detect reliably[9]. Among the many techniques that have been used for DNA amplification, polymerase chain reaction (PCR) remains to be the gold standard. However, PCR requires the use of multiple primers, DNA polymerases and high precision thermal cycling, and the need to identify and optimize specific working conditions can limit its use in routine and rapid DNA analysis in medical diagnostic laboratories. Moreover, PCR is also susceptible to contamination and amplification bias, limiting its detection and quantification accuracy. Hence, considerable efforts have been devoted to develop DNA sensing methods that can provide rapid, ultrasensitive SNP detection without the need of PCR amplification. This is particularly important for the early, non-invasive detection of cancer tumours before they metastasize uncontrollably and become incurable.

Over the past two decades, several methods capable of SNP detection and discrimination have been reported. These include high resolution DNA melting [10-12], single molecule fluorescence [13], molecular beacons [14, 15], hybridization chain reactions [16, 17], surface enhanced Raman scattering [18-21], and electrochemical detection [22, 23]. Despite well-designed strategies, most of these methods displayed either relatively low SNP discrimination and/or insufficient sensitivity, limiting their potential in real-world applications. While methods based on nicking endonucleases [24] or restriction enzymes [25] can offer high levels of SNP discrimination, these methods are limited to targets containing the specific enzyme recognition site only. On the other hand, ligase-based approaches are general and can work with any target of interest and offer high SNP discrimination.[26, 27] Moreover, it can be coupled to various signal amplification strategies, *e.g.* rolling circle amplification[28-30], polymerase mediated target displacement,[31-33] as well as nanomaterials to further improve sensitivity. In particular, coupling to magnetic nanoparticles (MNPs) are highly attractive because superparamagnetic MNPs can form stable, homogenous dispersions in the absence of an external magnetic field, allowing for rapid target capture and high enzymatic activity[34]; yet they are readily retrieved magnetically with an external magnetic field for easy removal of any unbound species to reduce background.[34b] Indeed, by combining target recycled ligation, MNP capture and enzymatic signal amplification, we have demonstrated the successful detection of specific target-DNAs down to the sub-pM level with high SNP discrimination,[35,36] although such sensitivities are

[a] *School of Chemistry and Astbury Centre for Structural Molecular Biology, University of Leeds, Leeds LS2 9JT, U.K. Email: d.zhou@leeds.ac.uk (D.Z.)*
[b] *Department of Chemical Engineering, Faculty of Engineering, University of Santo Tomas, España Boulevard, Manila, Philippines.*
[c] *School of Food Science and Nutrition and Astbury Centre for Structural Molecular Biology, University of Leeds, Leeds LS2 9JT, U.K. Email: y.guo@leeds.ac.uk (Y.G.)*
† Electronic Supplementary Information (ESI) available: The synthesis and spectroscopic characterisation of PEG-PMAO polymers and supporting figures. See DOI: 10.1039/x0xx00000x

still uncompetitive against some of the most recent ultrasensitive DNA detection methods.[37-40]

Building upon our earlier MNP-enzyme sandwich assay[36], herein we have introduced a direct MNP-signal-DNA ligation to increase the target-DNA to enzyme conversion efficiency. Moreover, we have developed a new poly-enzyme nanobead signal amplification strategy which can convert each captured target-DNA into thousands of copies of enzymes for greatly enhanced signal amplification power, allowing us to achieve ultrasensitivity and excellent SNP discrimination simultaneously. Given the importance of KRAS gene mutations in cancer detection,[41] we are motivated to develop a simple, rapid and ultrasensitive KRAS gene detection method. Moreover, since the KRAS somatic mutations (codons 12/13) are widely found in human cancers, (*e.g.* colorectal, pancreas, ductal, and lung),[35] we decided to use them as the model DNA targets to demonstrate the application of our new sensing strategy.

Experimental

DNA Probes and Reagents

All DNA probes used in this study were purchased from IBA GmbH (Germany). Their abbreviations and sequences are shown in Table S1 (see Supporting Information, ESI). High activity neutravidin-HRP conjugate (NAV-HRP) and amplex red were purchased from Thermo Scientific (UK) and Invitrogen Life Technologies (UK), respectively. *Taq* DNA ligase (40,000 U/mL) and 10× ligation buffer were purchased from New England Biolabs (UK). Methoxy-polyethylene glycol amine (NH_2-PEG_n-OCH_3, MW ~1000, n = ~23) was purchased from Alfa Aesar (UK). Dry powders of manganese iron oxide magnetic nanoparticles ($MnFe_2O_4$ MNPs, nominal diameter ~50 nm), poly(ethylene glycol) (M_n ~1000), poly(maleic anhydride-*alt*-1-octadecene) (PMAO, M_n = 30k-50k), dicyclohexylcarbodiimide (DCC), dimethylamino-pyridine (DMAP), methane sulfonyl chloride, NaN_3, triphenylphosphine, and bovine serum albumin (BSA) were purchased from Sigma Aldrich (UK). Amine modified polystyrene nanobead aqueous dispersion (~180 nm diameter, containing 2.54% solid by weight) was purchased from Bangs Laboratories, Inc. (USA). HABA Biotin Quantitation kit was purchased from Cambridge Bioscience (UK). Sterilized ultra-pure water (≥18.2 MΩ) generated by ELGA Purelab flex purification system was used throughout the experiments and to make buffer solutions (PBS: 20 mM phosphate, 150 mM NaCl, pH 7.4; PBS-tween: PBS containing 0.1% of tween 20).

Polymer Modification and Characterization

PMAO was modified with NH_2-PEG_n-N_3 (n = ~23) and NH_2-PEG_n-OCH_3 (n = ~23) in 30% and 70% grafting ratios respectively to form an amphiphilic PEG-PMAO polymer. The number of moles of the amino-PEG reagents were twice that the PMAO monomer unit. First, PMAO (0.250 g, 0.66 mmol monomer unit) was reacted with NH_2-PEG_n-N_3 (0.396 g, 0.396 mmol) in dry $CHCl_3$ under a N_2 atmosphere for 12 h. The remaining unreacted anhydride groups were reacted with NH_2-PEG-OCH_3 (0.923 g, 0.923 mmol) for 24 h. The solvent was removed and the crude polymer was dried under vacuum. The reaction flask was then sealed, purged with N_2 and placed in an ice bath. Dry $CHCl_3$ (5 mL) was added to dissolve the polymer followed by DCC (0.164 g, 0.792 mmol) and DMAP (0.014g, 0.11 mmol) dissolved in dry $CHCl_3$ at 0 ºC. The reaction mixture was allowed to gradually warm up to RT and stirred for 72 h. The DCC/DMAP coupling step was used to convert the carboxylic acids formed during the anhydride ring opening to amide linked-PEGs to increase PEG grating density. The reaction mixture was filtered and concentrated under vacuum to give a yellowish oil (~1.5 g). It was dissolved in $CHCl_3$ to make a ~100 mg·mL^{-1} stock and was used directly to encapsulate hydrophobic $MnFe_2O_4$ MNPs without purification, taking the full advantage of MNP's ease of magnetic retrieval for efficient removal of undesirable impurities.

MNP Encapsulation and Stability Evaluation

5.0 mg of $MnFe_2O_4$ MNPs were dispersed in 1.0 mL $CHCl_3$ though sonication, then different amount of the PEG-PMAO polymer was added (MNP:polymer weight ratio = 1:5, 1:10 and 1:15) and stirred overnight at RT. After that, ethanol was added to reach a 1:1 volume ratio with $CHCl_3$ and then $CHCl_3$ was slowly removed by rotary evaporation. The resulting MNP dispersion was transferred to a centrifugal filter (10000 MW cut-off) and water was added to a 1:1 v:v ratio and then centrifuged at 4000 rpm for 10 min. The MNPs were washed five times by centrifugation with water and finally dispersed in sterilized water to give a black solution. The solution was filtered through a 0.45 μm syringe filter to remove large aggregated particles. The MNPs were further centrifuged (14000 rpm, 15 min) and washed with water 3 times to remove any unbound polymers and other contaminants, and finally dispersed in pure water. Combining several different batches, a final MNP stock solution of ~10 mg·mL^{-1} was obtained. The MNP colloidal stability and hydrodynamic sizes at different temperatures (25-75 ºC) and salt contents were determined by dynamic light scattering (DLS)[42].

MNP-capture-DNA Conjugation

The copper-free "click" reaction between the MNP surface azide and DBCO-modified capture-DNA was employed for the capture-DNA-MNP conjugation. The PEG-PMAO encapsulated MNPs (10 mg) were mixed with the DBCO capture-DNA (100 μL, 100 μM) and incubated for 48 h at a constant 600 rpm vortex. After that, the MNPs were centrifuged and washed three times with pure water to remove any unbound capture-DNA. The clear supernatants were collected to determine the amount of unbound DNA. The capture-DNA loading was calculated from the difference between the amount of DNA added and that remained in clear supernatant as described previously[36].

Target Ligation and Enzymatic Assay

All sample tubes were pre-treated with PBS containing 1.0 mg·mL^{-1} of BSA to minimise non-specific adsorption. All ligation experiments were carried out with the MNP with a capture-DNA loading of ~0.35 nmol.mg^{-1} (MNP) by dispersing 30 μg of the MNP-capture-DNA (10 μL) to a tube containing 15 μL ultrapure water, 5 μL ligase buffer (10×), 10 μL target-DNA (different concentration), 10 μL signal-DNA (500 pM), and 1 μL Taq DNA ligase (10 U/μL). The samples were incubated at 45 ºC in a dry heating block for 60 min, after which they were cooled to RT naturally. The MNPs were centrifuged (3000 rpm) for 1 min and pulled to the tube wall *via* a permanent magnet. The clear supernatant was carefully removed, and the MNPs was washed twice with PBS-Tween. NAV-HRP (50 μL, 100 pM) was added and incubated for 60 min, after which the samples were centrifuged to remove the clear supernatant. The MNPs were washed four times with PBS-Tween, once with PBS and finally dispersed in PBS (80 μL) and transferred to 96 microplate wells. Each well was added amplex red (300 μM, 10 μL) and H_2O_2 (300 μM, 10 μL) to initiate enzymatic assays which was monitored by fluorescence time traces on an Envision® plate reader using BODIPY TMR FP 531 excitation filter and Cy3 595 emission filter. Ligation assays for SNP discrimination were performed in the same way by changing the target-DNAs.

Preparation of polymer nanobead (PB)-PEG_{12}-Biotin

An aqueous suspension of amino-functionalized polymer nanobeads (100 μL, 2.54 % weight) was centrifuged for 1 min at 15,000 g and the supernatant was discarded. The beads were washed twice with sodium bicarbonate buffer (20

mM $NaHCO_3$, pH 8.3), and then dispersed in 1.0 mL of sodium bicarbonate buffer (pH 8.3). NHS-PEG_{12}-Biotin (100 µL, 250 mM) was added to the nanobeads and incubated overnight at a rotor at 600 rpm at RT. The unreacted surface amino groups were further passivated by treatment with NHS-PEG_{750} (100 µL, 100 mM) to minimize non-specific adsorption. The resulting biotinylated polymer nanoparticles were centrifuged at 20,000 g and washed twice with PBS and finally dispersed in 5 mL of PBS.

Nanobead biotin valency determination and NAV-HRP tagging

The nanobead biotin loading was determined using HABA assay. An assay solution was prepared by adding avidin to HABA solution following the kit instruction and mixed for 5 minutes. 900 µL of the HABA/Avidin solution was added to a cuvette and its absorbance at 500 nm was measured. Then, a 100 µL biotin-modified polymer nanobeads was added and mixed by inversion several times. After removal of the polymer beads by centrifugation, the absorbance of the supernatant at 500 nm was measured. Using the method described in SI, S4, the biotin valency was determined as ~10^4 per nanobead. An equimolar amount of NAV-HRP to the bead surface biotin was then added to make up the poly-enzyme nanobead signal amplifier stock solution with a concentration of 0.50 µM (based on the NAV-HRP concentration, C_{HRP}).

Biosensing via poly-enzyme nanobead amplification

The MNP-capture-DNA and signal-DNA was mixed and ligated using the same procedures described above except much lower target-DNA concentrations (e.g. 0.001, 0.01, 0.1, 1, 10, 100 and 1000 fM) were used. After ligation, the samples were washed twice with PBS-Tween and then dispersed in 100 µL of the poly-enzyme nanobead signal amplifier in PBS (final C_{HRP} = 1.0 pM) and incubated for 60 min at RT. The samples were washed twice with PBS-tween and then transferred to a 96 well plate to initiate enzymatic assays as described above.

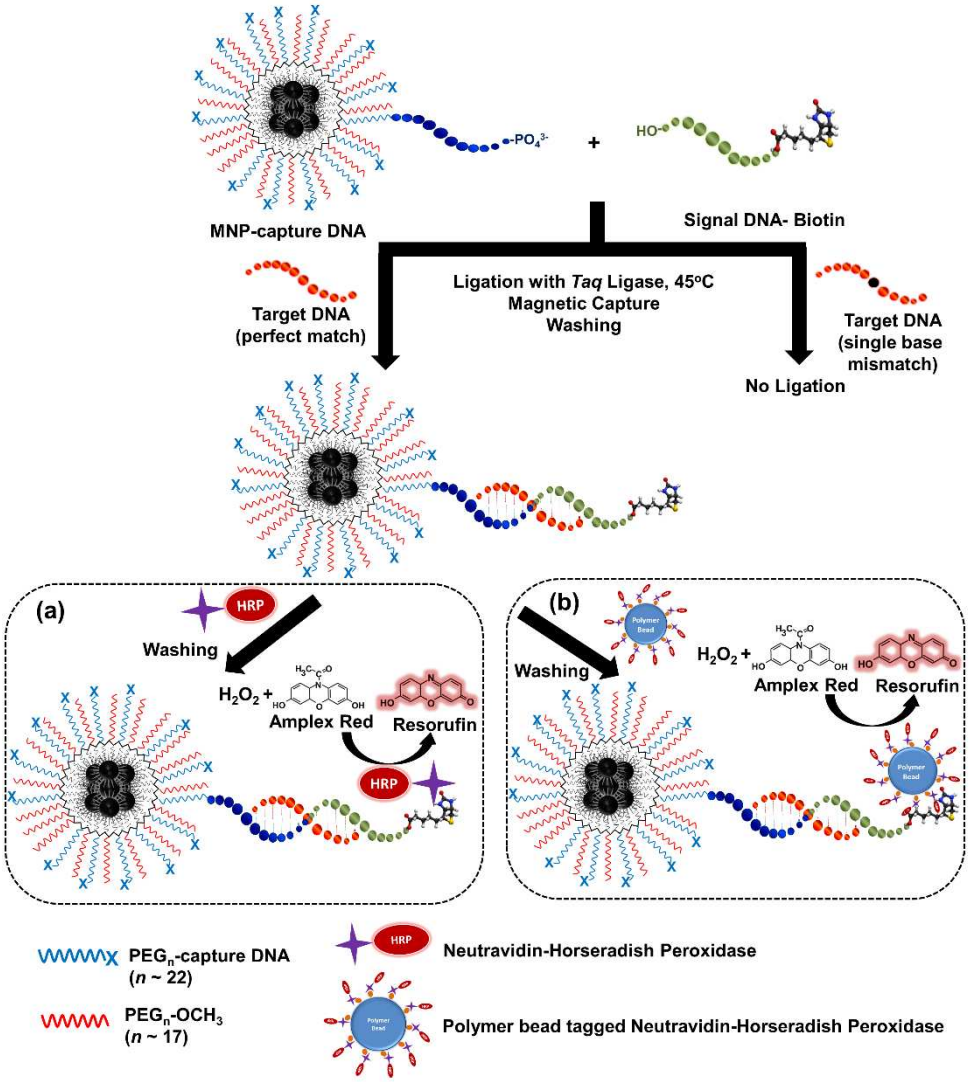

Scheme 1. Schematic Illustration of our DNA sensing strategy. A MNP linked capture-DNA and a biotinylated signal-DNA are used to sandwich hybridize with the target-DNA followed by ligation. Only the perfect-match target-DNA, but not the SNP target, can template the covalent ligation of the MNP-capture-DNA and signal-DNA, producing a MNP-linked biotin for binding to NAV-HRP (Route **a**) or poly-NAV-HRP polymer nanobead (Route **b**) for HRP catalysed enzymatic assay

Results and Discussion

Biosensing Principle

Our sensing principle is illustrated in Scheme 1. It uses a pair of DNA probes, one covalently linked to a MNP for target capture (*i.e.* capture-DNA, 5' phosphorinated), and the other (*i.e.* signal-DNA) is

biotinylated for NAV-HRP binding and signal amplification. The capture- and signal- DNA sequence are complimentary to each half of the target-DNA, allowing them to hybridize with a target-DNA to form nicked double-stranded DNA sandwich. It is noteworthy that in this study, a signal-DNA-Biotin design was used to hybridize with half of the sequence of the target-DNA rather than an enzyme labelled signal-DNA (*i.e.* signal-DNA-HRP). The small biotin in the signal-DNA would allow efficient hybridization with the target-DNA without inducing steric hindrance that may affect hybridisation or ligation.

A ligation step using *Taq* DNA ligase then covalently links the biotinylated signal-DNA to the capture-DNA (templated by a full-match target-DNA), ensuring that it will not detach from the MNP in the subsequent washing steps, thereby increasing the target-DNA to enzyme conversion (the nicked double-stranded DNA sandwich may dissociate during washing). It is important that the site of single-base mismatch is at the nicking double-stranded site to prevent ligation, thus, capture-DNA and target-DNA (*i.e.* SNP) remain unlinked. In this manner, the biosensor can effectively discriminate a perfectly matched target and a SNP target-DNA. After washing to remove any unbound species, NAV-HRPs (Route a) are added to bind to the MNP surface biotin, converting each MNP-ligated signal-DNA into a MNP-linked HRP for enzymatic fluorescence signal amplification[34]. The rate of fluorescence production is linear to the number of MNP surface HRPs, which is directly correlated to the full-match target-DNA concentration. To further improve sensitivity, a more powerful signal amplification strategy using poly-enzyme nanobeads, each tagged with thousands of copies of NAV-HRP, is designed (Route b). It can convert each successfully ligated signal-DNA into thousands of copies of HRPs for greatly improved sensitivity, allowing us to detect ultralow levels of target-DNA directly without PCR amplification. Moreover, the requirement of perfect-match to produce successful ligation also enables our approach to effectively discriminate between wildtype and cancer specific SNPs: a single base mismatch at the nicking double-stranded site can prevent covalent ligation.[35]

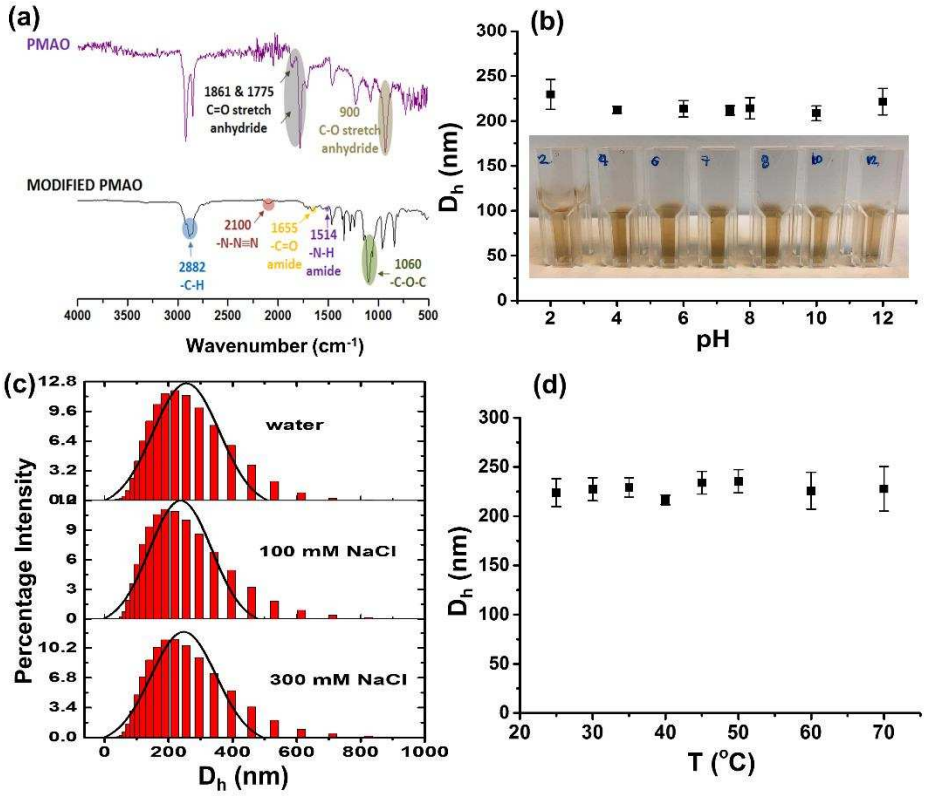

Figure 1. (**a**) FT-IR spectra of the unmodified (top) and PEG-modified PMAO (bottom) polymers. Comparison of the hydrodynamic diameters (D_hs) of the polymer encapsulated MNPs in water at different (**b**) pH, (**c**) NaCl content, and (**d**) temperature.

MNP dispersion and stability

Water dispersion of hydrophobic MNPs was achieved *via* PEG-PMAO-polymer encapsulation. PEG is used owing to its ability to resist the non-specific adsorption of biomolecules (*i.e.* proteins) and excellent biocompatibility.[43-45] Its flexible ether backbone utilizes hydrogen bonding and steric stabilization, and not electrostatic interactions, to achieve water dispersion. This confers PEG encapsulated or modified nanoparticles excellent colloidal stability in aqueous media over a wide range of pH and even with high salt contents. The maleic anhydride rings in PMAO was opened by reacting to amino-PEG molecules (*i.e.* NH_2-PEG-N_3), forming a carboxylic acid and an amide linked-PEG-N_3. The generated free carboxylic acid was further reacted with NH_2-PEG-OCH_3 *via* DCC/DMAP mediated amide coupling to increase the PEG graft density, forming a dense, brush like PEG structure for excellent hydrophilicity and resistance against non-specific adsorption.[42]

Fig. 1(a) showed the FT-IR spectra of the unmodified PAMO and PMAO-PEG copolymers. The original PMAO gave a strong peak at 1775 cm^{-1}, assigning to the C=O stretching of the anhydride ring.[46] This peak was completely diminished after modification, indicating a complete reaction of the anhydride functional groups. The opening of the anhydride ring was also confirmed by the appearance of the

amide C=O stretching peak at 1655 cm^{-1} and amide N-H bending peak at 1514 cm^{-1}. Moreover, the appearance of the azide stretching peak at 2100 cm^{-1} as well as the -C-O-C- absorption at 1060 cm^{-1} clearly demonstrated the successful grafting of the NH_2-PEG-N_3. The azide moiety was used to conjugate DBCO-modified capture-DNA *via* the efficient copper-free click chemistry. The C-H stretching peaks of the alkyl chains at 2882 and 2930 cm^{-1} remained unchanged. These alkyl chains can interact with the hydrophobic ligands on the MNP surface *via* van der Waals interactions, leaving the hydrophilic PEG moieties exposed to the aqueous media to confer particle water-dispersity.

The prepared PMAO-PEG copolymer was used directly to disperse hydrophobic $MnFe_2O_4$ MNPs using a modified solvent exchange method reported by Bao and colleagues.[47] First, ethanol was added to a chloroform solution containing the MNP and PEG-PMAO polymer in 1:1 volume ratio. Then chloroform was selectively removed by rotary evaporation, and finally, ethanol was replaced by water using centrifugal filter tubes (10k MW cut off). During this process, the solvent polarity increased gradually from chloroform to water to improve encapsulation efficiency. The resulting MNPs was found to be highly stable, showing no signs of precipitation after storage at RT for >6 months.

The amounts of the PMAO-PEG for MNP encapsulation was optimized by varying the polymer:MNP weight ratios from 5:1 to 15:1. MNP dispersed at 5:1 gave a much fainter colour as compared to those prepared at 10:1 or 15:1 (ESI, Fig. S1), indicating that this ratio was insufficient to promote high MNP water-dispersion. In contrast, those dispersed at 10:1 and 15:1 were similar in colour and much darker than that of 5:1, suggesting these ratios provided high MNP encapsulation efficiency. The encapsulation efficiency at each polymer: MNP ratio was further determined after removing the supernatant containing polymer encapsulated MNP, the precipitated MNPs were washed 3 times to remove excess polymer and then dried in an oven for 3 days and their weights were determined. The weight difference between the initial MNP and that remained in the precipitate was considered as polymer encapsulated. Using this method, the polymer encapsulation efficiency was calculated as 39, 56 and 53 % for the polymer:MNP ratio of 5:1, 10:1, and 15:1, respectively, suggesting that maximum encapsulation efficiency was achieved at 10:1.

The primary goal here was to make stable MNP dispersions in high yields using the minimal amount of polymer possible, hence 10:1 was determined to be optimal. The hydrodynamic diameters (D_hs) of the polymer encapsulated MNPs were found to be ~230 nm by dynamic light scattering. Such relatively large D_h sizes were likely due to MNP clustering as revealed by TEM imaging (ESI, Fig. S1) and bilayer formation: the polymer alkyl chains interact with the hydrophobic ligands on the MNP surface *via* hydrophobic interactions.[48] It should be noted that the commercial MNPs were supplied as dry powders which were heavily aggregated and were hardly dispersible even in organic solvents (e.g. $CHCl_3$) prior to polymer encapsulation. Thus encapsulation of the PMAO-PEG polymer significantly reduced the MNP aggregation, allowing them to disperse stably in water. Moreover, no significant D_h size variations were observed for the polymer encapsulated MNPs prepared in different batches.

The colloidal stability of the MNPs under different temperature, salt content, and pH were further investigated. Fig. 1b showed that the MNPs did not display any significant D_h size variations over a wide pH range (*i.e.* 2-12). Furthermore, no precipitation was observed over a period of 7 days (Fig. 1b inset). The MNPs were stable under different salt contents (*e.g.* 100, 300 mM NaCl) with similar D_hs as those dispersed in pure water (Fig. 1c). These results suggested that the MNPs were not mainly stabilized by electrostatic repulsion otherwise significant D_h increase would have been expected in high salt media. The high MNP colloidal stability was attributed to effective steric stabilisation afforded by a thick hydrophilic PEG coating, preventing the MNPs from interaction with each other.[49-51] Since the ligation step will be carried out at 45 °C, the thermal stability of the MNPs was further tested. As shown in Fig. 1d, no significant MNP size changes were found from 25 to 70 °C, suggesting that the PMAO-PEG provided a stable coating for the MNP, presumably *via* multiple hydrophobic interactions between the polymer alkyl chains and MNP surface hydrophobic ligands.[52] The attachment of the PMAO-PEG co-polymer to the MNP surface can be viewed as "irreversible" in an aqueous environment, making such MNPs capable of withstanding relatively harsh conditions.

Optimization of capture-DNA loading

We have previously found that increasing capture-DNA loading on silica coated MNPs can increase the target-DNA capture efficiency, presumably *via* enhanced binding affinity.[36] However, too high a capture-DNA loading can lead to high background signals, possibly due to non-specific interactions.[36] Therefore, the MNPs with different capture-DNA loading (e.g. 0.04, 0.10, 0.20, and 0.35 $nmol{\cdot}mg^{-1}$) were prepared to investigate the optimal loading. The MNPs (30 μg each) were mixed with the signal-DNA and full-match target-DNA (10 pM each) followed by ligation and NAV-HRP binding. A control without the target-DNA (WOT) was also prepared under identical conditions. The typical time-dependent fluorescence response curves and the corresponding slopes were shown in Fig. S2 (ESI). The highest signal was obtained for the MNP having the highest capture-DNA loading (e.g. 0.35 $nmol{\cdot}mg^{-1}$), while those having the capture-DNA loading of 0.04 and 0.10 $nmol{\cdot}mg^{-1}$ were rather low and comparable to the control. Unfortunately, we were unable to prepare MNPs with the capture-DNA loadings higher than 0.35 $nmol{\cdot}mg^{-1}$, hence this loading was used in all subsequent sensing experiments. All subsequent DNA sensing experiments *via* the Route (a) were carried out with a fixed 100 pM signal-DNA in PBS. The assay gave a steady increase of fluorescence with time (Fig. S3, ESI). The signal was highest for the highest target-DNA concentration (10 pM) and decreased with the decreasing target-DNA concentration with the control giving the lowest signal as expected. The limit of detection (LOD) based on three times the standard deviation plus the negative control signal (*i.e.* $LOD = 3\sigma_{WOT} + I_{WOT}$) [30, 53] was determined as 1.0 pM. This LOD is comparable to a more intricate electro-chemical DNA sensing using a DNA tetrahedron structure[3]. In general, a main drawback of surface based assays is the reduced accessibility of target molecules to surface immobilized probes compared to binding in solution.[54, 55] Moreover, inert spacers are often needed to passivate the surface to reduce non-specific adsorption and block vacant spaces to allow the capture-DNA probes adopting an upright position to favour hybridization. Here capture-

DNA was conjugated to the MNP surface *via* a long chain PEG linker (~23 EG units). The surface was further blocked by an inert PEG$_{\sim 23}$-OCH_3 to minimise non-specific adsorption, making the capture-DNA oriented toward the solution to achieve high hybridization efficiency.[56] As a result, this simple design of polymer encapsulated MNP coupled to DNA sandwich hybridization has achieved a LOD comparable to many previously reported DNA sensors (e.g. nM-pM sensitivity, see ESI, Table S2) without target amplification and more sophisticated designs. However, the 1 pM LOD is still uncompetitive against some of the recent ultrasensitive DNA assays (ESI, Table S3) [57-60]. Thus a more powerful signal amplification strategy was designed to further improve sensitivity (see later section).

SNP discrimination

The sensor was further evaluated for its ability to detect specific SNPs in the KRAS gene associated with many human cancers (*e.g.* colorectal, pancreas, ductal and lung). Here three target-DNAs (all 10 pM) were employed: wild-type T1 (counting from 5', base 17 → C), two cancer mutants: T2 (17C → T) and T3 (17C → A). The sensing was done in PBS and PBS containing 10% human serum to mimic clinical assay conditions. Fig. 2a revealed that only the full-match target-DNA (T1, see Fig. 2 below) produced a high fluorescence response, the signals for both SNP targets (T2, T3) were practically the same as background, *i.e.* this sensor was highly specific. The SNP discrimination ratio (ratio of the fluorescence production rate) for T1 against the SNP targets before background correction was determined as ~14.3 and 16.8 for T2 and T3, respectively. This level of SNP discrimination is comparable or better than many other assays reported in the literature.[6-8, 61, 62] Moreover, even higher SNP discrimination ratios (*ca.* 33, without background correction) were obtained in clinically relevant media (e.g. PBS containing 10 % human serum, see Fig. 2b), demonstrating that our sensor is highly robust and work effectively under clinically relevant conditions. The relatively large error bars for the perfect-match (T1/S1) samples were most likely due to the rather small amount of MNPs used in each assay (30 μg), making it challenging to completely remove the non-bound enzymes without removing any MNPs. This was often encountered for assays using very small amount of the MNPs (as per experience). Nonetheless, each sample was performed in triplicates and the experiment was repeated three times, all giving very similar results. Moreover, the signals for the T1/S1 combination, despite relatively large error bars, were always significantly higher than those of the single-base mismatch (T2/S1, T3/S1) and WOT samples, and thus the data presented herein were reliable for drawing a valid conclusion.

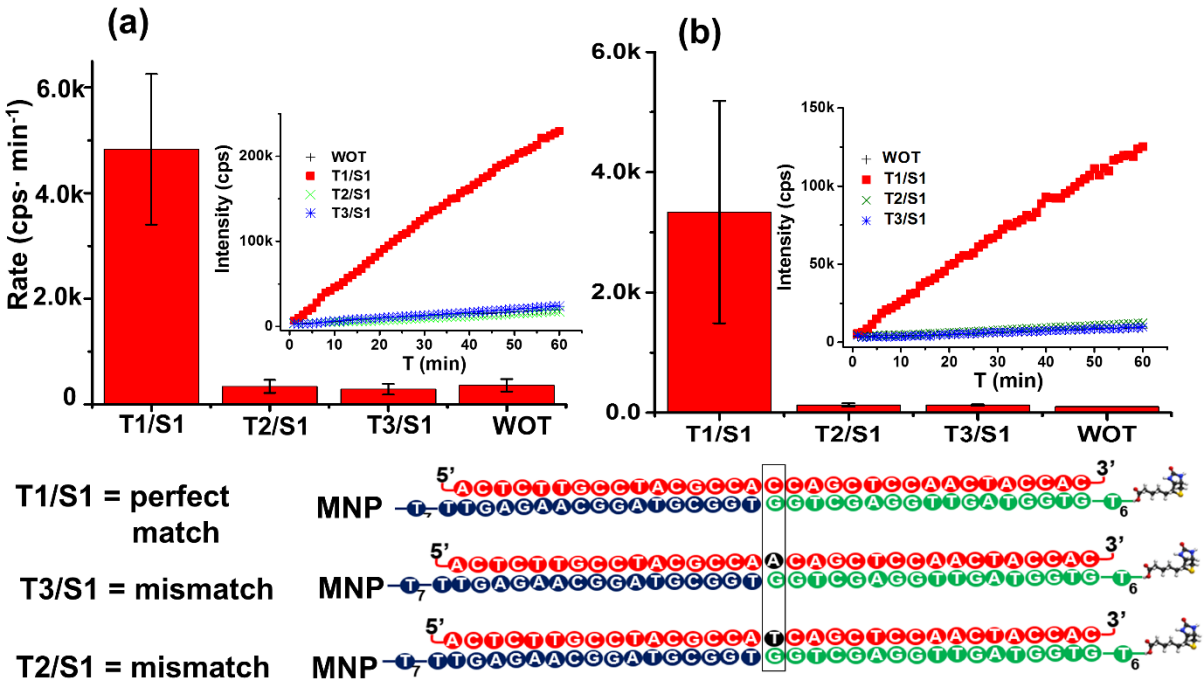

Figure 2. Discrimination of the perfect-match DNA (T1) against other SNP targets (T2 and T3). (**a**) Comparison of the average fluorescence production rates (slopes of fluorescence response curves shown in inset) for different DNA targets in PBS (**a**) or PBS containing 10% Human serum (**b**, *n* = 3).

Poly-enzyme nanobead amplification

A more powerful signal amplification strategy using poly-enzyme nanobeads each tagged with ~10^4 copies of NAV-HRPs was designed to further improve sensitivity (Scheme 1, Route b). We first prepared NHS-EG_{12}-biotin modified polymer nanobeads, determined its biotin loading valency as ~10^4 per bead, and then conjugated the nanobead with NAV-HRP by incubating with 1:1 mole ratio of NAV-HRP to the bead surface biotin. The MNP-capture-DNA and signal-DNA were mixed with different amounts of target-DNA, and ligated as above and then treated with poly-enzyme nanobead. The resulting time-dependent fluorescence response curves were shown in Fig. 3(a) inset. The highest signal was observed for the 1 pM target-DNA sample as expected. A very low fluorescence signal was observed from the control sample (no target-DNA), suggesting that the polymer encapsulated MNP was highly effective in resisting non-specific adsorption. Here a low background is critical to achieve high

sensitivity, allowing for unambiguous detection of weak signals arising from ultralow levels of target molecules. As shown in Fig. 3b, our sensing strategy provided a rather wide linear dynamic range (rate of fluorescence intensity increase *v.s.* $\log C_{DNA}$) of 6 orders of magnitude (*e.g.* 1 aM to 1 pM, R^2 = 0.966) with a LOD of as 1.6 aM based on the interception point between the linear fit and the background + 3σ level. Such levels of sensitivity place it among the most sensitive DNA biosensors reported in the literature (see ESI, Table S3). We attribute the ultrasensitivity obtained here to the greatly increased signal amplification power of the poly-enzyme nanobead, each carrying ~10^4 copies of HRPs. As a result, it may be able to convert each captured full-match target-DNA into ~10^4 copies of HRPs (*versus* 1 in the traditional sandwich assay) for greatly enhanced sensitivity. Together with our elaborately designed surface chemistry and PEGylated coatings which effectively resist non-specific adsorption, leading to greatly reduced background and hence allowing us to achieve ultrasensitivity.

Although ultrasensitive DNA sensors have been reported previously via elaborately designed signal and/or target amplification strategies, our sensing strategy reported herein is simple (*via* incubation with a poly-enzyme nanobead), straightforward (direct detection without target pre-amplification), and compatible with conventional plate reader systems for rapid, high throughput detection, yet it still can offer low aM sensitivity which is among the best reported in literature. The ability to detect target directly can be especially beneficial to situations (*e.g.* clinical samples) where target pre-amplification may not be always feasible. Moreover, our poly-enzyme nanobead signal amplifiers can be easily and reliably prepared by incubating NAV-HRP with PEGylated biotin nanobeads. Furthermore, the poly-enzyme nanobeads can be used as powerful signal amplifiers in other bioassays such as ELISA to broaden its application scope. To the best of our knowledge this is the first report on using a poly-enzyme nanobead as signal amplifier for ultra-sensitive detection of cancer related DNA targets.

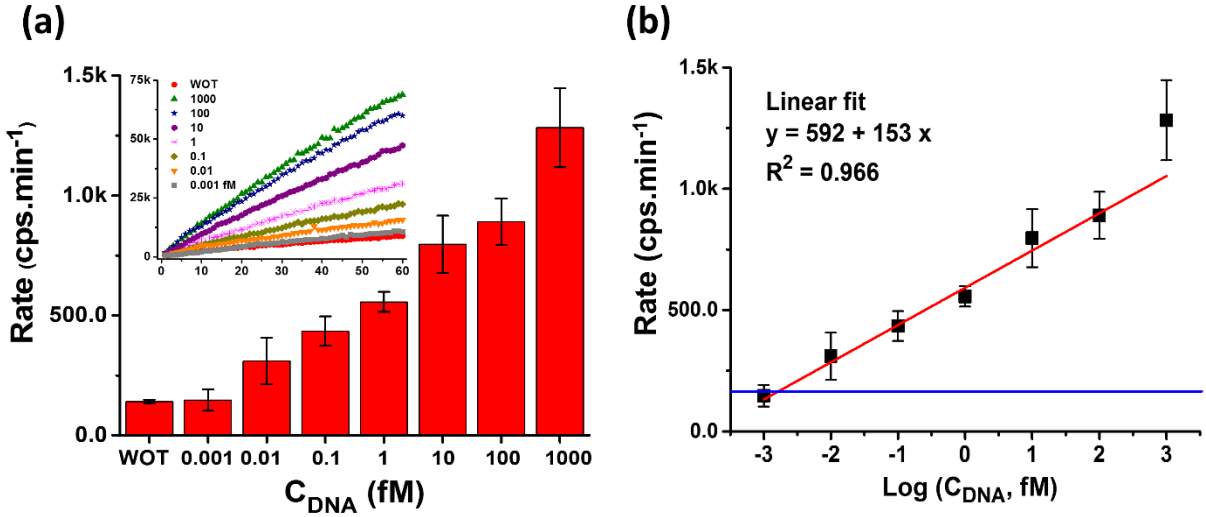

Figure 3. (**a**) Comparison of the average fluorescence increase rate (cps·min^{-1}) for assays containing 0-1000 fM of T1 (inset show the corresponding time-dependent fluorescence responses, n = 3). (**b**) Relation between the fluorescence increase rate and the log(C_{DNA}, in fM) fitted by a linear function (y = 153x + 592, r^2 = 0.966). The blue line shows the background + 3σ level which intercepts with the linear fit at x = -2.788, corresponding to C_{DNA} = 1.6 aM.

Besides ultra-sensitivity, the ability to accurately and reliably detect low abundant specific SNPs in a background of wildtype genes is of great importance for the non-invasive diagnosis of cancer and other diseases.[63] Therefore the ability of our sensing strategy to detect low abundance full-match target-DNA (T1) in large excess of SNP targets (T2 and T3) was also investigated. The final DNA concentrations were 1 fM for the full-match T1 and 10 fM (*i.e.*10-fold excess) or 100 fM (*i.e.* 100-fold excess) for each SNP target (T2 and T3). Fig. 4 revealed that, increasing the SNP:T1 ratio led to a decreased fluorescence signal, presumably because the large excess of SNP targets (T2 or T3) could compete with T1 to sandwich hybridize to the capture- and signal- DNAs, reducing the chances of a successful ligation templated by the full-match T1. Nevertheless, the signal of samples containing just 1 fM T1 (1% that of the T2/T3 SNP target concentration) is clearly higher than those of the SNP targets only, suggesting that our sensor can specifically detect 1 fM full-match target even in the presence of

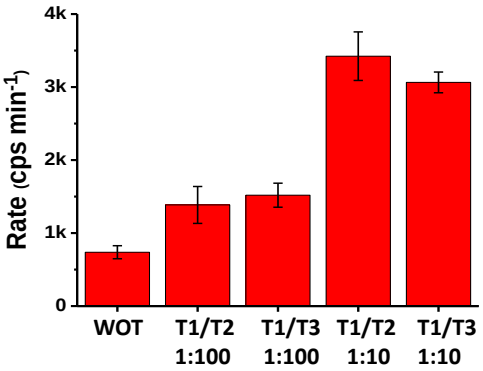

Figure 4. Detection of 1 fM of the perfect-match T1 in the presence of large excess (10 or 100 fold) of the SNP targets (T2, T3). WOT: a control with 100 fM of T2 and T3 each but without T1.

100 fold excess of SNP targets. This level of specificity for the perfect-match target-DNA over its SNP targets is among the very best SNP sensors reported in literature.[57, 64] We also noticed that impressively

high SNP discrimination ratios (up to 10000) were reported with an DNA tetrahedron based electrochemical sensor, but this level of SNP discrimination was achieved at a target-DNA concentration of 1 nM,[3] 6 orders of magnitude higher than the 1 fM concentration reported herein. Despite significant research over the past two decades, the ability to achieve simultaneous ultra-sensitivity (e.g. low aM levels of LOD) and high SNP discrimination remained challenging in direct target-DNA detection without PCR pre-amplification. Although in the proof of principle experiments, the signal-DNA probe was designed to be fully complementary to T1 (wildtype), and not to T2 or T3 (cancer related SNP targets), to demonstrate the ultra-sensitivity and exclusive selectively for the perfect-match over other single-base mismatch targets of this sensing method. Given the universally high specificity of the DNA ligation assay for the full-match over single-base mismatch targets as we have demonstrated previously,[35] designing a signal-DNA sequence that matches perfectly to T2 or T3 should allow for specific detection of such cancer related SNP targets in potential clinical diagnostic applications which will be carried out in the following on work.

Conclusions

We have shown that encapsulation of hydrophobic MNPs with an azide-PEG functionalised amphiphilic polymer not only produces stable, well-dispersed MNPs that effectively resist non-specific adsorption, but also enables the convenient DNA conjugation *via* Cu-free "click" chemistry. A new sensing strategy based on sandwich hybridisation followed by ligation to introduce biotins on the MNP surface for subsequent enzymatic amplification has yielded excellent SNP discrimination. Moreover, a new powerful signal amplification strategy using a poly-enzyme nanobead which can convert each captured target-DNA into thousands of copies of enzymes has been developed, enabling the direct detection of target-DNA down to 1.6 aM with a linear dynamic range of 6 orders of magnitude, placing it among the most sensitive PCR-free DNA sensors. Furthermore, this sensor is highly robust (works effectively in clinically relevant media) and specific (can positively detect 1% of the full-match target in a background of 100 fold excess SNP targets), suggesting that it may have broad applications in biosensing and clinical diagnostics. Future work will focus on extending this method to ultrasensitive detection of cancer related SNPs and explore its application in clinical samples.

Conflicts of interest

There are no conflicts of interest to declare.

Acknowledgements

We thank Dr. Nicole Hondow (School of Chemical and Process Engineering, University of Leeds) for help in collecting the TEM images of the MNPs and the University of Leeds for funding this project. L.DS.L thanks the University of Leeds for providing a Leeds International Research Scholarship (LIRS) to allow him study at University of Leeds.

Notes and references

1. F. Xia, R. J. White, X. Zuo, A. Patterson, Y. Xiao, D. Kang, X. Gong, K. W. Plaxco and A. J. Heeger, *J. Am. Chem. Soc.*, 2010, **132**, 14346-14348.
2. T. Wu, W. Chen, Z. Yang, H. Tan, J. Wang, X. Xiao, M. Li and M. Zhao, *Nucleic Acids Res.*, 2018, **46**, Art. No e24.
3. H. Pei, N. Lu, Y. Wen, S. Song, Y. Liu, H. Yan and C. Fan, *Adv. Mater.*, 2010, **22**, 4754-4758.
4. D. Zhang, M. C. Huarng and E. C. Alocilja, *Biosens. Bioelectron.*, 2010, **26**, 1736-1742.
5. Y. Xiang and Y. Lu, *Anal. Chem.*, 2012, **84**, 1975-1980.
6. H. Liu, S. Li, L. Liu, L. Tian and N. He, *Biosens. Bioelectron.*, 2010, **26**, 1442-1448.
7. X. Duan, Z. Li, F. He and S. Wang, *J. Am. Chem. Soc.*, 2007, **129**, 4154-4155.
8. X. Xiao, C. Zhang, X. Su, C. Song and M. Zhao, *Chem. Sci.*, 2012, **3**, 2257-2261.
9. F. Diehl, M. Li, D. Dressman, Y. He, D. Shen, S. Szabo, L. A. Diaz, S. N. Goodman, K. A. David and H. Juhl, *Proc. Natl. Acad. Sci. USA.*, 2005, **102**, 16368-16373.
10. G. H. Reed, J. O. Kent and C. T. Wittwer, *Pharmacogenomics*, 2007, **8**, 597-608.
11. U. Malapelle, C. Carlomagno, M. Salatiello, A. De Stefano, C. De Luca, R. Bianco, R. Marciano, C. Cimminiello, C. Bellevicine and S. De Placido, *Br. J. Cancer.*, 2012, **107**, 626-631.
12. S. Sorgenfrei, C.-y. Chiu, R. L. Gonzalez Jr, Y.-J. Yu, P. Kim, C. Nuckolls and K. L. Shepard, *Nat. Nanotechnol.*, 2011, **6**, 126-132.
13. I. I. Cisse, H. Kim and T. Ha, *Nat. Struct. Mol. Biol.*, 2012, **19**, 623-627.
14. B. Liu, S. Baudrey, L. Jaeger and G. C. Bazan, *J. Am. Chem. Soc.*, 2004, **126**, 4076-4077.
15. J. Grimes, Y. V. Gerasimova and D. M. Kolpashchikov, *Angew. Chem. Int. Ed.*, 2010, **49**, 8950-8953.
16. J. Huang, Y. Wu, Y. Chen, Z. Zhu, X. Yang, C. J. Yang, K. Wang and W. Tan, *Angew. Chem. Int. Ed.*, 2011, **50**, 401-404.
17. P. Liu, X. Yang, S. Sun, Q. Wang, K. Wang, J. Huang, J. Liu and L. He, *Anal. Chem.*, 2013, **85**, 7689-7695.
18. S. He, K.-K. Liu, S. Su, J. Yan, X. Mao, D. Wang, Y. He, L.-J. Li, S. Song and C. Fan, *Anal. Chem.*, **2012**, **84**, 4622-4627.
19. M. Li, S. K. Cushing, H. Liang, S. Suri, D. Ma and N. Wu, *Anal. Chem.*, 2013, **85**, 2072-2078.
20. L. B. Sagle, L. K. Ruvuna, J. A. Ruemmele and R. P. Van Duyne, *Nanomedicine*, 2011, **6**, 1447-1462.
21. E. Papadopoulou and S. E. Bell, *Angew. Chem. Int. Ed.*, 2011, **50**, 9058-9061.
22. L. Qiu, L. Qiu, Z. S. Wu, G. Shen and R. Q. Yu, *Anal. Chem.*, 2013, **85**, 8225-8231.
23. L. Qiu, L. Qiu, H. Zhou, Z. Wu, G. Shen and R. Yu, *New J. Chem.*, 2014, **38**, 4711-4715.
24. W. Xu, X. Xue, T. Li, H. Zeng and X. Liu, *Angew. Chem. Int. Ed.*, 2009, **48**, 6849-6852.
25. W. Li, P. Wu, H. Zhang and C. Cai, *Anal. Chem.*, 2012, **84**, 7583-7590.
26. Z. Zou, Z. Qing, X. He, K. Wang, D. He, H. Shi, X. Yang, T. Qing and X. Yang, *Talanta*, 2014, **125**, 306-312.
27. Y. Chen, M. Yang, Y. Xiang, R. Yuan and Y. Chai, *Anal. Chim. Acta*, 2013, **796**, 1-6.
28. S. Zhang, Z. Wu, G. Shen and R. Yu, *Biosens. Bioelectron.*, 2009, **24**, 3201-3207.

29. M. M. Ali, F. Li, Z. Zhang, K. Zhang, D. K. Kang, J. A. Ankrum, X. C. Le and W. Zhao, *Chem. Soc. Rev.*, 2014, **43**, 3324-3341.
30. Y. Long, X. Zhou and D. Xing, *Biosens. Bioelectron.*, 2013, **46**, 102-107.
31. Z. Zhang, D. Zeng, H. Ma, G. Feng, J. Hu, L. He, C. Li and C. Fan, *Small*, 2010, **6**, 1854-1858.
32. D. Wang, W. Tang, X. Wu, X. Wang, G. Chen, Q. Chen, N. Li and F. Liu, *Anal. Chem.*, 2012, **84**, 7008-7014.
33. A. Chen, G.-F. Gui, Y. Zhuo, Y.-Q. Chai, Y. Xiang and R. Yuan, *Anal. Chem.*, 2015, **87**, 6328-6334.
34. a) J. Garcia, Y. Zhang, H. Taylor, O. Cespedes, M. E. Webb and D. Zhou, *Nanoscale*, 2011, **3**, 3721-3730; b) Y. Zhang and D. Zhou, *Expert. Rev. Mol. Diagn.*, 2012, **12**, 565-572.
35. Y. Zhang, Y. Guo, P. Quirke and D. Zhou, *Nanoscale*, 2013, **5**, 5027-5035.
36. Y. Zhang, C. Pilapong, Y. Guo, Z. Ling, O. Cespedes, P. Quirke and D. Zhou, *Anal. Chem.*, 2013, **85**, 9238-9244.
37. J. Lei and H. Ju, *Chem. Soc. Rev.*, 2012, **41**, 2122-2134.
38. J. Wang, *Small*, 2005, **1**, 1036-1043.
39. Y. Chai, D. Tian, W. Wang and H. Cui, *Chem. Commun.*, 2010, **46**, 7560-7562.
40. J. Li, S. Song, D. Li, Y. Su, Q. Huang, Y. Zhao and C. Fan, *Biosens. Bioelectron.*, 2009, **24**, 3311-3315.
41. C. J. Allegra, J. M. Jessup, M. R. Somerfield, S. R. Hamilton, E. H. Hammond, D. F. Hayes, P. K. McAllister, R. F. Morton and R. L. Schilsky, *J. Clin. Oncol.*, 2009, **27**, 2091-2096.
42. a) L. Song, V. H. Ho, C. Chen, Z. Yang, D. Liu, R. Chen and D. Zhou, *Adv. Healthc. Mater.*, 2013, **2**, 275-280. b) Y. Guo, I. Nehlmeier, E. Poole, C. Sakonsinsiri, N. Hondow, A. Brown, Q. Li, S. Li, J. Whitworth, Z. Li, A. Yu, R. Brydson, W. B. Turnbull, S. Pöhlmann and D. Zhou, *J. Am. Chem. Soc.*, 2017, **139**, 11833-11844. c) Y. Guo, C. Sakonsinsiri, I. Nehlmeier, M. A. Fascione, H. Zhang, W. Wang, S. Pöhlmann, W. B. Turnbull and D. Zhou, *Angew. Chem. Int. Ed.*, 2016, **55**, 4738-4742.
43. K. Knop, R. Hoogenboom, D. Fischer and U. S. Schubert, *Angew. Chem. Int. Ed.*, 2010, **49**, 6288-6308.
44. D. Zhou, A. Bruckbauer, L. Ying, C. Abell and D. Klenerman, *Nano Lett.*, 2003, **3**, 1517-1520.
45. L. Song, Y. Guo, D. Roebuck, C. Chen, M. Yang, Z. Yang, S. Sreedharan, C. Glover, J. A. Thomas, D. Liu, S. Guo, R. Chen and D. Zhou, *ACS Appl. Mater. Interfaces*, 2015, **7**, 18707-18716.
46. E. Peng, E. S. G. Choo, Y. Sheng and J. M. Xue, *New J. Chem.*, 2013, **37**, 2051-2060.
47. S. Tong, S. Hou, B. Ren, Z. Zheng and G. Bao, *Nano Lett.*, 2011, **11**, 3720.
48. E. E. Lees, T.-L. Nguyen, A. H. Clayton and P. Mulvaney, *ACS Nano.*, 2009, **3**, 1121-1128.
49. M. M. Yallapu, S. P. Foy, T. K. Jain and V. Labhasetwar, *Pharm. Res.*, 2010, **27**, 2283-2295.
50. W. S. Seo, J. H. Lee, X. Sun, Y. Suzuki, D. Mann, Z. Liu, M. Terashima, P. C. Yang, M. V. McConnell and D. G. Nishimura, *Nat. Mater.*, 2006, **5**, 971.
51. J. Shin, R. M. Anisur, M. K. Ko, G. H. Im, J. H. Lee and I. S. Lee, *Angew. Chem. Int. Ed.*, 2009, **48**, 321-324.
52. M. Moros, B. Pelaz, P. López-Larrubia, M. L. García-Martin, V. Grazú and M. Jesus, *Nanoscale*, 2010, **2**, 1746-1755.
53. a) D. M. Rissin, C. W. Kan, T. G. Campbell, S. C. Howes, D. R. Fournier, L. Song, T. Piech, P. P. Patel, L. Chang and A. J. Rivnak, *Nat. Biotechnol.*, 2010, **28**, 595-599. b) W. Wang, Y. Guo, C. Tiede, S. Chen, M. Kopytynski, Y. Kong, A. Kulak, D. Tomlinson, R. Chen, M. McPherson and D. Zhou, *ACS Appl. Mater. Interfaces*, 2017, **9**, 15232-15244.
54. D. Irving, P. Gong and R. Levicky, *J. Phys. Chem. B*, 2010, **114**, 7631-7640.
55. I. Y. Wong and N. A. Melosh, *Biophys. J.*, 2010, **98**, 2954-2963.
56. E. L. Wong, E. Chow and J. J. Gooding, *Langmuir*, 2005, **21**, 6957-6965.
57. D. Kato and M. Oishi, *ACS Nano*, 2014, **8**, 9988-9997.
58. H.-L. Shuai, K.-J. Huang and Y.-X. Chen, *J. Mater. Chem. B.*, 2016, **4**, 1186-1196.
59. F. Zhou, B. Li and J. Ma, *RSC Adv.*, 2015, **5**, 4019-4025.
60. H. T. Ngo, N. Gandra, A. M. Fales, S. M. Taylor and T. Vo-Dinh, *Biosens. Bioelectron.*, 2016, **81**, 8-14.
61. Y. Song, W. Zhang, Y. An, L. Cui, C. Yu, Z. Zhu and C. J. Yang, *Chem. Commun.*, 2012, **48**, 576-578.
62. Y. Cheng, Q. Du, L. Wang, H. Jia and Z. Li, *Anal. Chem.*, **2012**, **84**, 3739-3744.
63. D. Dressman, H. Yan, G. Traverso, K. W. Kinzler and B. Vogelstein, *Proc. Natl. Acad. Sci. USA.*, 2003, **100**, 8817-8822.
64. W. Shen, H. Deng and Z. Gao, *J. Am. Chem. Soc.*, 2012, **134**, 14678-14681.

Graphical abstract

An ultrasensitive sensor which combines magnetic capture and poly-enzyme nanobead amplification to quantify low aM DNA target is developed.